

Quantification of deuterium irradiation induced defect concentrations in tungsten

T. Ahlgren^{a,*}, K. Heinola^a, E. Vainonen-Ahlgren^b, J. Likonen^b, J. Keinonen^a

^a Accelerator Laboratory, University of Helsinki, P.O. Box 64, FIN-00014 Helsinki, Finland

^b VTT Processes, Association EURATOM-Tekes, P.O. Box 1608, FIN-02044 VTT, Finland

Available online 2 May 2006

Abstract

Tungsten has been proposed for first wall material in thermonuclear reactors, where its behaviour in the presence of hydrogen containing plasma irradiation at elevated temperatures is of key interest. Deuterium induced defects in polycrystalline tungsten have been studied. Deuterium was implanted into tungsten samples and retained D-concentrations were analyzed with nuclear reaction analysis and secondary ion mass spectrometry. We observed four different defect types that trap deuterium with release temperatures of 455, 560, 663 and 801 K. Total number of each defect type produced by $5.8 \times 10^{16} \text{ cm}^{-2}$ 30-keV D implantation at room temperature was obtained to be 0.260, 0.156, 0.082 and 0.056 traps cm^{-2} /implanted D atom.

© 2006 Elsevier B.V. All rights reserved.

PACS: 25.55.Ci; 61.18.Bn; 61.80.Jh; 66.30.Jt

Keywords: Defect; Deuterium; Tungsten; NRA; SIMS

1. Introduction

In fusion reactors, hydrogen escaping the plasma can cause hydrogen build-up in the sub-surface region of first wall materials. This captured hydrogen can also be released back to the plasma. This retention and release of hydrogen, also called recycling, will influence the particle balance in the plasma. Furthermore, the build-up or also called the inventory of tritium in the first walls and divertor areas is an important environmental issue to be considered for long time fusion operation.

Tungsten is a strong candidate as plasma facing material in fusion machines. It has high melting point, good thermal conductivity and low sputtering yields. As a drawback, once sputtered to the plasma, the W particles cause great power losses and plasma contamination.

Retention and re-emission of hydrogen isotopes in tungsten have been studied extensively in the literature [1–7]. Hydrogen has a relatively low diffusion activation energy of 0.39 eV in body centred cubic (bcc) W [8]. Thus, the very fast diffusion of hydrogen at room temperature results in that only hydrogen trapped in intrinsic and ion implantation induced defects are present in the sample. The initial displacements of atoms from their lattice sites in metals during ion irradiation is quite accurately known using computer simulations along with binary collision approximation and molecular dynamics methods [9]. However, due to migration of vacancies and interstitials, recombination and clustering of defects occurring during implantation in second time scales, the final number and concentrations of defects are not known. Furthermore, the similarity of implanted atom and defect depth profiles indicate that defects can also be stabilized by the implanted atoms.

To understand and predict plasma conditions, besides experiments, different plasma and plasma surface interaction programs are used. These codes need a lot of

* Corresponding author. Tel.: +358 9 19150648; fax: +358 9 19150042.
E-mail address: tommy.ahlgren@helsinki.fi (T. Ahlgren).

parameters including the number of different hydrogen trapping types, and their concentration profiles.

In many previous studies, the hydrogen implantation energy has been so low that no accurate hydrogen or defect profiles could be measured.

The aim of this work is thus to determine number and concentration profiles for defects that trap hydrogen. To achieve this, the deuterium implantation energy has been chosen to be 30 keV per deuterium (D) ion, in order to make the depth profile measurements for hydrogen traps possible.

2. Experimental

High purity (99.99%) polycrystalline W sheet (thickness of 1 mm) produced by Plansee AG (Reutte Austria) was used. The sheet was cut into pieces ($15 \times 10 \text{ mm}^2$) which were mirror-polished with colloidal silica (grain size of $\sim 0.05 \mu\text{m}$). A 3D stylus profilometer (KLA-Tencor P-15 Profiler) was used to measure the surface roughness, which was less than 10 nm root mean square. The samples were pre-annealed at about 1370 K for 2 h a priori implantation in order to reduce the grain boundaries within the samples.

The polished tungsten samples were implanted at room temperature (RT) with 60-keV D_2^+ ions (30 keV per deuterium) perpendicular to the surface in a vacuum of $\sim 10^{-8}$ mbar. The implantation dose was $5.8 \times 10^{16} \text{ D/cm}^2$, which corresponds to a maximum D concentration of 5 at.% if all the deuterium would have retained in the implanted range profile. The quite low implantation fluence was chosen to avoid blister formation on the sample surface. Also a reference sample for calibrating the D concentrations was prepared by implanting 30-keV D_2^+ ions to a fluence of $7.5 \times 10^{16} \text{ D/cm}^2$ into silicon.

Annealing was carried out in a quartz-tube furnace equipped with a quadrupole mass spectrometer (QMS). The temperature was measured with a calibrated thermocouple in direct contact with the sample surface. During annealing of the sample, the D_2 partial pressure varied between 10^{-12} and 10^{-10} mbar, while the total pressure in the chamber was less than 10^{-7} mbar.

The as-implanted and annealed D concentration profiles were measured with secondary ion mass spectrometer (SIMS) and nuclear reaction analysis (NRA) technique. In this work, due to the low D implantation dose used, the good depth resolution of SIMS was combined with the quantitative NRA method to obtain accurate D depth profiles.

The SIMS measurements were done using 12 keV cesium primary ions. The primary ion current was 150 nA and analyzed area $290 \times 430 \mu\text{m}^2$. Crater wall effects were avoided by using a 10% electronic gate and 2 mm optical gate. The pressure inside the analysis chamber was 5×10^{-10} mbar during the analysis. The depth of the craters was measured by a profilometer (Dektak 3030ST). The uncertainty of the crater depth was estimated to be 10%.

The NRA measurements were carried out using the $\text{D}({}^3\text{He}, \text{p}){}^4\text{He}$ nuclear reaction which has a relatively broad

differential cross-section peak of $\sim 60 \text{ mb/sr}$ near 640 keV ${}^3\text{He}$ energy [10,11]. At ${}^3\text{He}$ energies below 1.2 MeV the differential cross-section is angle independent [11–13]. A 700-keV ${}^3\text{He}^{2+}$, 0.5 mm in diameter collimated beam at 40° incident angle from the sample normal was used. A $650 \mu\text{m}$ Mylar foil was put in front of the $700 \mu\text{m}$ silicon detector to stop the ${}^4\text{He}$ from the reaction and to slow down the 13.7 MeV protons emitted from the $\text{D}({}^3\text{He}, \text{p}){}^4\text{He}$ reaction. The solid angle of the detector, placed at 60° to the incident beam, was 0.1 sr and the wide 20° aperture of the detector allowed protons with reaction angle between 110° and 130° and corresponding energies between ~ 14.0 and ~ 13.3 MeV to enter the detector.

Proton energy straggling of about 100 keV in the Mylar foil, together with the ~ 300 keV kinematic broadening due to the large detector solid angle used, did not have any effect in the analysis of the spectra since only the total number of counts in the proton peak area were of interest. The calibration of the SIMS depth profiles were done using the SIMNRA computer program [14]. SIMS D depth distributions were used in the programme and the height of the D concentration was then varied until the calculated proton yield matched the experimental ones. The ${}^3\text{He}^{2+}$ ion charge was calibrated using a D implanted silicon standard together with a beam chopper system. In addition, the QMS data was checked with a calibrated D_2 leak bottle and the deviation from NRA calibration was less than 7%.

3. Results and discussion

To study defects that trap D in W, we annealed D implanted samples in different temperatures and measured the desorption of D_2 molecules from W surface. Fig. 1 shows the initial part of the annealing temperature and QMS signal as a function of annealing time. Due to the high mobility of D atoms, only trapped D is left in the sample after RT implantation. Each defect type, hereafter called simply trap, has different D binding energy, which is defined as the energy difference for a D atom in a trap compared to a solute or mobile atom in the crystal. To distinguish different traps from each other, we performed the annealing so that when D started to detrapp from a trap, the temperature was kept constant in order to remove all D from that particular trap. This can be seen in Fig. 1, where D release from the first trap started at temperature of about 455 K. During this annealing, the maximum temperature of about 528 K was too low to see any D release from the second trap, which starts at temperature 560 K. The sample temperature was kept at about 528 K until the QMS-signal dropped to zero and all D atoms from the first trap was removed.

To obtain the concentration profiles for the different D traps, the as-implanted and annealed samples were measured with SIMS and NRA techniques. Fig. 2 presents the depth profiles of D atoms for each sample measured by SIMS and normalized by NRA. The areas for the collected proton NRA spectra were over 2000 counts, giving

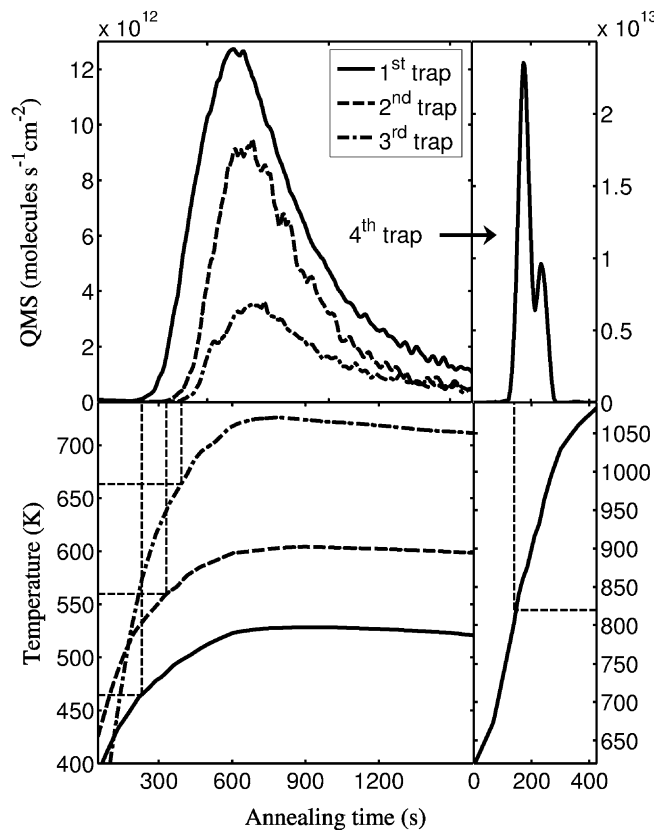


Fig. 1. D_2 molecule thermodesorption spectra and annealing temperatures as a function of annealing time for removing D atoms from four different traps in W. D release starts at sample temperatures 455, 560, 663 and 801 K from traps 1 to 4, respectively.

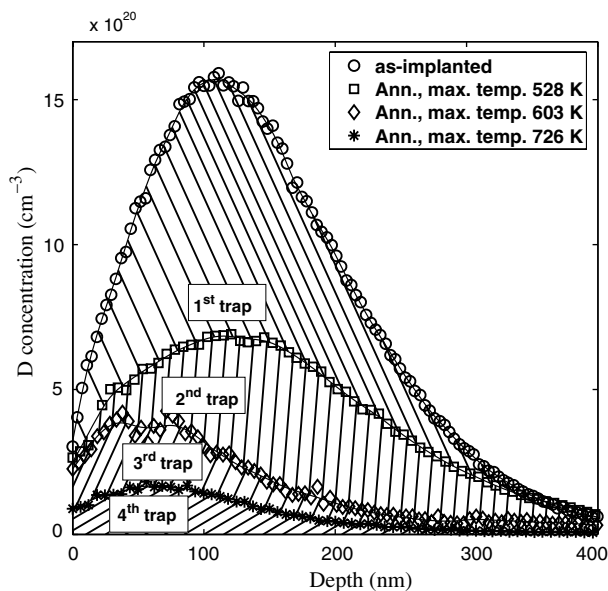


Fig. 2. As-implanted and annealed D depth profiles measured by SIMS and normalized with NRA. The different striped regions show profiles of each trap type.

the statistical uncertainty of about 2% to the profile areas. The collected rotor counts to normalize collected charge

for each measurement exceeded 100,000 counts, adding no significant error to the measurements. The D concentration profile was obtained by comparing proton yields from W sample and D implanted Si standard. Therefore, some uncertainty is added concerning the accuracy of the ^3He stopping powers in W and Si. This systematic error is the same for all W samples and the ratios of the concentration profiles should be quite unaffected by the possible stopping power error. The total accumulated ion charge per sample was about $50 \mu\text{C}$, which did not alter the D concentration in the sample, confirmed by repeated measurements. Also a second detector was placed at near glancing angle to obtain D depth profiles by monitoring the ^4He from the reaction as used by Alimov et al. [15]. The low D concentration in the sample together with the very small solid angle needed to avoid kinematic broadening resulted in an unfortunately low countrate, rendering depth profile determination this way impractical.

Fig. 2 shows not only the concentration profiles of D, but also the profiles of D traps. Annealing at temperature 528 K removes all D atoms from the first trap, illustrated by the area between as-implanted and 528 K annealed profiles. To check that all D from the 1st trap is removed, the sample was re-annealed at the same temperature and time, during which no QMS-signal from desorbed D_2 molecules was observed and no change of the concentration profile compared with the one prior the additional annealing was detected in post mortem SIMS measurements either.

The retained D in the as-implanted profile is 3.22×10^{16} at. cm^{-2} , being about 55% of the implanted fluence. From this amount, about 47% of D is released during the first annealing procedure. Second and third annealing at the maximum temperatures of 603 and 726 K removed additionally about 28% and 15% from the initial amount, respectively. The final annealing up to the temperature of 1100 K removed finally the rest 10% of the remaining D, right part of Fig. 1.

The 5.8×10^{16} D cm^{-2} , 30-keV/D implantation produced totally at least 3.22×10^{16} D traps/ cm^2 . The integrated numbers of the four different types of defect created and their D release temperatures are given in Table 1. Fig. 3 shows depth profiles of each individual trap, from Fig. 2, together with the vacancy distribution simulated by SRIM-03. The vacancy distribution is the sum distribution of vacancies produced by D ions and by recoil W calculated using Kinchin–Pease estimate [16]. In the figure, it

Table 1
Different trap parameters resulting from 5.8×10^{16} D cm^{-2} 30-keV/D atom implantation

	Defects/ cm^2	Temperature where release starts (K)
1st	1.5×10^{16}	455 ± 5
2nd	9.1×10^{15}	560 ± 2
3rd	4.8×10^{15}	663 ± 2
4th	3.3×10^{15}	801 ± 20

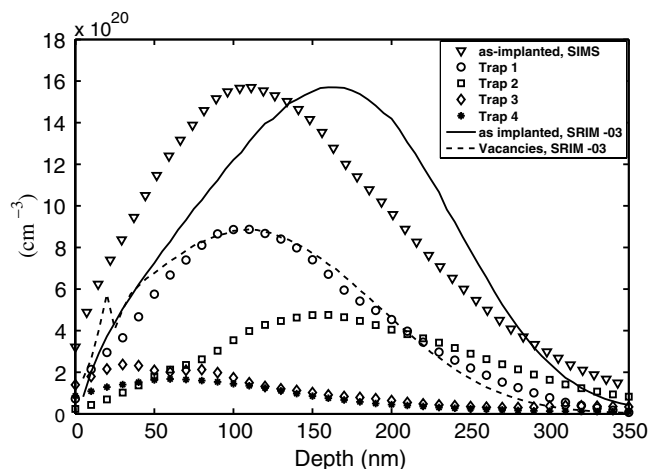


Fig. 3. Depth profiles of experimental and simulated SRIM-03 profiles. The as-implanted SRIM-03 profile has been divided by a factor of 1.7 to make the height same as for the the experimental one. The SRIM-03 vacancy distribution has been divided by a factor of 55, to match the maximum trap 1 concentration. Most of the initially formed vacancies and interstitials recombine anyway during and shortly after implantation.

is seen that the distribution of the first trap matches the implantation produced vacancy profile. Thus, the first D trap in bcc W could be associated with a vacancy, which was also the conclusion derived by Myers et al. studying D trapping in bcc Fe using ion channeling technique [17].

Trap 2 extending deeper into the sample, could be explained by ion beam studies by Nagata et al. [18] and transmission electron microscopy studies by Matsui et al. [19]. They show that traps can be associated with lattice distortion due to implantation induced extended defects of interstitial type. D implantation produces strain in the bulk, which is relieved by W interstitial loops, which can be distributed far deeper than expected from D implantation range and to which D atoms are trapped. The remaining D traps with larger binding energy shown in Fig. 3 are probably associated with defect clusters.

Fig. 3 further illustrates that SRIM-03 simulation of as-implanted distribution overestimates the depth at maximum concentration with about 45%. Looking at projected ranges and widths, the difference is less due to the deep extending D tail for the experimental profile, SRIM-05: $R_p = 157$ nm, $\Delta R_p = 72$ nm, Experimental: $R_p = 150$ nm, $\Delta R_p = 103$ nm.

The present study has shown that at least four D traps with different binding energies exist in irradiated W. Further experiments with lower D implantation energies are still needed for extrapolation to fusion relevant energies. Further, in future attempts to determine accurate binding energies for D traps, following considerations should be taken into account. Present numerical desorption models use sub-surface bulk D concentration, which should be

replaced with the physically correct surface areal D concentration. Secondly, the surface areal D concentration depends critically on the energy barriers for D atoms to jump from bulk to surface and surface to bulk. To our knowledge, no values for these important surface parameters can be found in the literature.

4. Conclusion

Deuterium irradiation in tungsten results in at least four D traps with different binding energies. From the 30-keV RT implanted D fluence of 5.8×10^{16} D cm⁻², only about 3.2×10^{16} D atoms cm⁻² are trapped in the near surface implantation region in a profile resembling the SRIM-03 simulated implantation induced damage profile. Annealing releases D atoms gradually from the traps, resulting in D-molecule desorption from the surface. When the sample temperature reaches about 1100 K, no D is left in the vicinity of the surface. The similarity of the first D trap profile with the SRIM-03 vacancy profile, makes it tempting to associate the first trap with irradiation induced vacancies. The traps which can be distributed far deeper than expected from D implantation range, are associated with lattice distortion due to implantation induced extended defects of interstitial type.

Acknowledgement

This work was supported by the Association EUR-ATOM-Tekes.

References

- [1] R.A. Anderl et al., Fusion Technol. 21 (1992) 745.
- [2] A.A. Haasz et al., J. Nucl. Mater. 258–263 (1999) 75.
- [3] R. Causey et al., J. Nucl. Mater. 266–269 (1999) 467.
- [4] A.A. Haasz, M. Poon, J.W. Davis, J. Nucl. Mater. 266–269 (1999) 520.
- [5] A.A. Haasz et al., J. Nucl. Mater. 290–293 (2001) 85.
- [6] V. Kh. Alimov et al., Phys. Scripta T 94 (2001) 34.
- [7] V. Kh. Alimov, Phys. Scripta T 108 (2004) 46.
- [8] R. Frauenfelder, J. Vac. Sci. Technol. 6 (1969) 388.
- [9] R.S. Averback, J. Nucl. Mater. 216 (1994) 49.
- [10] W.E. Kunz, Phys. Rev. 97 (1955) 456.
- [11] W. Möller, F. Besenbacher, Nucl. Instr. and Meth. 168 (1980) 111.
- [12] J.L. Yarnell, R.H. Lovberg, W.R. Stratton, Phys. Rev. 90 (1953) 292.
- [13] T.W. Bonner, J.P. Conner, A.B. Lillie, Phys. Rev. 88 (1952) 456.
- [14] M. Mayer, SIMNRA's User's Guide, Tech. Rep. IPP 9/113, Max-Planck-Institut für Plasmaphysik, Garching, 1997.
- [15] V.Kh. Alimov, J. Roth, M. Mayer, Nucl. Instr. and Meth. B 168 (2005) 169.
- [16] G.H. Kinchin, R.S. Pease, Prog. Phys. 18 (1955) 1.
- [17] S.M. Myers, S.T. Picraux, R.E. Stoltz, J. Appl. Phys. 50 (1979) 5710.
- [18] S. Nagata, K. Takahiro, S. Horiike, S. Yamaguchi, J. Nucl. Mater. 266–269 (1999) 1151.
- [19] T. Matsui, S. Muto, T. Tanabe, J. Nucl. Mater. 283–287 (2000) 1139.